Moroccan Journal of Chemistry
ISSN : 2351-812X

Mor. J. Chem., 2023, Volume 11, Issue 3, Page 699-717
https://revues.imist.ma/index.php/morjchem
https://doi.org/10.48317/IMIST.PRSM/morjchem-v11i3.40613

Effect of heat treatment on bioelectronic coordinates and antibacterial activities of natural and synthetic clays

Zerhouni J. [1*], Rhazi Filali F. [1], Naciri Bennani M. [2], Houssaini J. [2]

[1]*Microbiology and health team: laboratory of Chemistry Biology applies to the environment, Faculty of Sciences, Moulay Ismail, Meknes University, Morocco.*

[2]*Materials and applied Catalysis team: laboratory of Chemistry Biology applied to the environment, Faculty of Sciences, Meknes, Morocco.*

**Corresponding author, Email address: boumnihi_jaouad@hotmail.com*

Received *05 June 2023,*
Revised *26 June 2023,*
Accepted *28 June 2023*

Citation*: Zerhouni J., Rhazi Filali F., Naciri Bennani M., Houssaini J. (2023) Effect of heat treatment on bioelectronic coordinates and antibacterial activities of natural and synthetic clays, Mor. J. Chem., 14(3), 699-717*

Abstract: Our work consists in studying the effect of the thermal treatment at 900°C of three clays "two anionic clays of synthesis ' Double lamellar hydroxide' $Zn_3Al\text{-}CO_3$ and $Mg_3Al\text{-}CO_3$, and another natural cationic: Ghassoul (Gh)", on their antibacterial and bioelectronic power. Their chemical characteristics such as pH at zero charge point (pH_{zcp}), redox potential (Eh), index of oxidizing/reducing power (rH2), and electrochemical potential to dissipate energy (W), as well as the type of oxide formed as a result of this treatment; were also determined. The materials were characterized by powder X-ray diffraction (XRD), Fourier transform infrared spectrometry (FTIR), and scanning electron microscopy (SEM). Antibacterial activity was tested for four bacteria: two Gram positive (*Staphylococcus aureus, Enterococcus faecalis*) and two Gram negative (*Escherichia coli, Salmonella spp*). The antibacterial power of the three clays was evaluated by their minimum inhibitory concentration (MIC) and minimum bactericidal concentration (MBC), using the microtiter plate technique. The results showed that the pH_{zcp}, rH2, W and antibacterial power of the two lamellar double hydroxides increased as a result of heat treatment. While the test on the heat treated cationic clay showed an opposite result. It thus appears that the changes in the physicochemical and electrochemical characteristics of the clays following their calcination at 900°C; are at the origin of the change in their antibacterial power.

Keywords: Clays; calcination; bioelectronic coordinates; Antibacterial

1. Introduction

The search for new substances with antibacterial activity as alternatives to conventional antibiotics is a very important and crucial scientific issue. For this reason, several studies have focused on clay materials because of their abundance in nature or their ease of synthesis and also for their important chemical and biological properties. (Reichle, 1986; Cavani *et al*., 1991; Kim *et al*., 1998; Vaccari, 1998; Benhammou *et al*., 2009; Ainane *et al*., 2021). The clay material Ghassoul (Gh) has aroused the interest of many chemists since the last century, it is a natural Moroccan cationic clay rich in magnesium, of majority phase smectite, (Belamine, 2012). The double lamellar hydroxides which are anionic clays, not very abundant in nature but which can also be obtained by synthesis in a great variety of composition, their oxidation-reduction or acid-base behavior and their electrical properties (Faure

et al., 1991; Demourgues-Guerlou & Delmas, 1994); give them interesting properties opening the prospect of their application in many fields: catalysis, environment, food industry, pharmaceutical industry, polymer industry and solid electrochemistry (Newman & Jones, 1999; Toraishi *et al.*, 2002; Nawal, 2015). To characterize the electronic activity of the studied clay materials, the specific power (W) of the materials was calculated. This one does not characterize the state of thermodynamic equilibrium, but it becomes a variable measuring a state of electrochemical potentiality to dissipate energy. A difference of W between two electrolytic media in contact becomes a kinetic factor of energetic contribution necessary to the maintenance of the structure (Országh, 1992). The chemical concept of rH2 was introduced in this work. Indeed, rH2 allows to evaluate the strength of an oxidant (or a reducer) by identifying the electron transfers alone (Fougerousse, 1996). The redox potential Eh, zero charge point, and resistivity of the materials were measured. In the light of what has just been presented, our interest in this work concerned the materials 'Ghassoul and LDH', raw and thermally treated at 900°C, in order to study their antibacterial activity according to their bioelectronic coordinates and the change of their physicochemical compositions.

2. Methodology

2.1 Sourcing and preparation of materials

The materials used in this study are two lamellar double hydroxides based on zinc and aluminum (Zn_3Al-CO_3), and the other based on magnesium and aluminum (Mg_3Al-CO_3). The cationic clay used is Ghassoul; from Jbel Ghassoul in the Fez-Meknes region of Morocco. The three materials were used raw and calcined at 900°C. Double lamellar hydroxide were synthesized by co-precipitation, (Miyata, 1975, Thenevot *et al*., 1989; Chang *et al*., 2005). This method consists in preparing an aqueous solution containing a mixture of NaOH (0.25 M) and Na_2CO_3 (0.05M) and another solution containing a mixture of two metal, with a molar ratio (Zn/Al, Mg/Al) equal to three. Co-precipitation was induced by adding the two solutions dropwise into a flask containing 20 ml of distilled water to maintain pH = 10. Then the mixture was kept under magnetic stirring at a temperature of 70°C for 18 h until crystallization. The precipitated product was filtered and washed several times with distilled water to remove excess ions (Cl^-, Na^+...), then dried at 105°C for 18 h (Rives, 2001; Qabaqous *et al*., 2018; Zerhouni *et al*., 2021). Ghassoul is a commercial sample (Ghassoul Chorfa Al Akhdar), it was crushed without any treatment. After drying it at 100°C, it was crushed and sieved with standardized sieves according to AFNOR with diameter between 250 and 315 µm (Qabaqous *et al*., 2014; Qabaqous *et al*., 2018 ; Zerhouni *et al*., 2019, Zerhouni *et al*., 2021). The products were characterized using XRD, FTIR, and SEM-EDX.

2.2 Product characterisation

Infrared analysis of the different materials was performed using a Schimadzu Model IRAffinity S Fourier Transform Spectrometer (FTIR), equipped with a detector (TGS) and a ceramic source. Absorption spectra were performed with pellets containing 1 mg sample and 100 mg KBr, and recorded in the interval 4000-400 cm^{-1}, with a resolution of 4 cm^{-1}.

Powder X-ray diffraction (XRD) analysis of the different materials was recorded using a Philips PW 1800 diffractometer (copper Kα line λ = 1.5406 Å, 40 kV, 20 mA) in Bragg-Brentano geometry. The spectra of the different samples were recorded in a 2θ range between 5° and 70° with an angular increment of 0.04°. The different analyses were performed at the Laboratory of Chemistry --Biology Applied to the Environment, Faculty of Sciences Meknes.

Scanning electron microscopy (SEM) was used to observe the morphology of the studied clays. Energy dispersive X-ray spectroscopy (EDX) is a characterization technique coupled with scanning electron microscopy, which can give the atomic composition on surfaces of the order of nanometer diameter. The various analyses were conducted at the Center for Innovation and Technology Transfer (CITT) of Moulay Ismail University, the device used is type JSM - IT 500 H R.
The calcined materials were noted as Gh-900, Zn_3Al-900, and Mg_3Al-900. Calcination was performed in a Nabertherm furnace for duration of four hours and a temperature of 900°C. Temperature and duration previously used by Velu *et al*., (1997) and Abderrazek *et al*., (2016). The different materials were characterized by XRD, IR and SEM.

2.3 Bioelectronics coordinates of the studied clays

Electrochemistry is concerned with the movement and transfer of charges from one medium to another. The ultimate unit of charge is the electron (Crow, 1994).
There are three bioelectronics coordinates: pH; rH_2 and electrical resistivity designated by the symbol ρ. If the measurement of pH allows to know the activity of hydronium ions (H_3O^+), the knowledge of the electronic balance imposes the consideration of the activity of molecular hydrogen (H_2), whose cologarithm is called rH_2, is defined as follows: $rH_2 = \log\left(\frac{1}{[H_2]}\right)$; where $[H_2]$ is the thermodynamic activity of molecular hydrogen that would be formed as a result of electron exchange between water and solutes (Országh, 1992). The calculation of the rH_2 value is done from the experimental measurement of the redox potential Eh and the pH, according to the following formula (Olivier *et al.*, 2015):

$$rH_{2(\text{at } 25°C)} = 33.3\ Eh_{(\text{volts})} + 2pH$$

The third bioelectronics coordinate, the electrical resistivity ρ in ohms.cm, is the inverse of the specific conductivity (σ) of the clay suspensions studied. It is expressed in micro-Siemens, and was measured by a Cond 340i / SET type conductivity meter, with $\rho = 1/\sigma$. Indeed, any redox system can be schematized using a cell consisting of a normal hydrogen electrode and an electrode containing the studied redox system in solution. The maximum power W of this cell is (Országh, 1992):

$$W = \frac{A \times (rH2 - 2pH)2}{\rho} = \frac{A \times (Eh)2}{\rho}$$

- ✓ A is a constant whose numerical value is 875 at 25°C
- ✓ Eh is the electromotive force (or free enthalpy to the nearest constant) of the battery.
- ✓ W in microwatts, ρ is the resistivity in ohms.cm.

The term W thus expresses the maximum rate of energy dissipation by a chemical or biochemical charge-transfer reaction in the broadest sense of the term, since the potential Eh depends on both the pH and rH_2 of the medium, since the term ρ appears in the expression for W.
The determination of the redox potential and pH of clays was carried out according to the method described by Longchambon (1939). Five g of clay were suspended in 100 ml of distilled water. The suspension was stirred for one hour to obtain an equilibrium between clay and water, then the Eh potential (expressed in mVolts) and pH were measured using conventional electrodes (pH meter Adwa AD1000). The measurements were carried out under the same conditions for all tested materials, with three repetitions.

2.4 Zero charge point (pH_{zcp})

The pH of the zero charge point (pH_{zcp}), corresponds to the pH value for which, the net charge of the adsorbent surface is zero (Nandi *et al*., 2009). It is interesting to know the zero charge point which corresponds to the state of equality between positive and negative charges on the surface of the clay. The presence of OH^- and H^+ ions in the solution can modify this charge potential at the surface of the material (Elyahyaoui *et al*, 2017; Azha *et al*., 2018). The pH_{zcp} was determined by putting 50 ml of a NaCl solution (0.01 M) in six closed vials, then their pH is adjusted to values of 2, 4, 6, 8, 10 and 12, by adding of NaOH or HCl (0.1 M) (Sahoo *et al*., 2014). Fifty mg of the material was then added to each vial. The suspensions were kept under agitation at room temperature for 24 hours. The final values of pH (pH_f) were subsequently recorded. The pH_{zcp} value is the point where the curve ΔpH ($pH_f - pH_i$) versus pH_i intersect the x-axis pH_i (Nandi *et al*., 2009; Shah *et al*., 2015; Boumchita *et al*., 2016).

2.5 Antibacterial tests

2.5.1 Preparation of clays

The solutions studied at 50 mg/ml concentrations, were prepared in suspension in the distilled water and mechanically agitated by vortex, then sterilized in an autoclave at 121°C for 20 minutes.

2.5.2 Germs tested and their origins

The antibacterial activity of the different materials was tested for two Gram+ bacteria: *Staphylococcus aureus* (*S. aureus*), *Enterococcus faecalis* (*EF*), and two Gram- bacteria: *Escherichia coli* (*E.coli*) and *Salmonella spp* (*Sal*). These bacteria were provided by the team of Microbiology and Health of the Laboratory of Chemistry Biology Applied to the Environment of the University Moulay-Ismail at the Faculty of Sciences of Meknes, Morocco.

2.5.3 Preparation of inoculums

Cultures of the bacteria were grown on nutrient agar (Mueller-Hinton) for 18 to 24 hours and incubated at 37°C. Then, these cultures were suspended in saline solution (0.9% NaCl) and inoculated respecting a density equivalent to McFarland standard density 0.5 or an absorbance included between 0.08 and 0.13 at 625 nm, which corresponds to an inoculums of approximately 1 to 210^8 CFU/ml (CASFM, 2021). The concentration of the inoculums used for the antibacterial test was 5 10^5 CFU/ml (Eloff, 1998; Andrews, 2001).

2.5.4 Determination of minimum inhibitory concentration (MIC)

The minimum inhibitory concentration was determined by the microdilution method on 96-well microplates. A volume of 50 µl of Mueller-Hinton broth was added to each well. Then, to the first well was added a volume of 50 µl of a tested clay suspension of concentration 50mg /1ml (this is the same concentration used for determination of redox potential and pH of the materials); from which a series of dilutions at a rate of 2 across the line was made until the tenth well. Then 50 µl of the bacterial suspension (with a concentration of 5.10^5 CFU/ml) was added to each well, followed by a 100µL volume of Mueller-Hinton broth added to each well. Well n°11 and n°12 are the positive and negative controls for bacterial growth, respectively. After incubation at 37±2°C for 24 hours, the reading is taken by adding 40 µl of TTC (2, 3, 5-triphenyltetrazohum chloride), which is used as a microbial viability indicator following a 30-minute incubation at 37±2°C; the red color in the wells indicates bacterial growth. Each test was repeated three times (Eloff, 1998; Andrews, 2001; Wade *et al*., 2001 ; Chebaibi *et al*., 2016 ; Jahanpanahi, 2016 ; Rasouli *et al*., 2017).

2.5.5 Determination of minimum bactericidal concentration (MBC)

Referring to the results of the MIC assay, the wells showing complete absence of bacterial growth were identified, and 10 µl of each well were transferred to Mueller-Hinton agar plates and incubated at 37°C for 24 h. The complete absence of growth was considered as the minimum bactericidal concentration (Zegaoui *et al*., 2014). Effect was determined according to the value of the CMB / MIC ratio. When the CMB/CMI ratio is greater than or equal to 4, the material tested is considered to be a bacteriostatic agent, if on the other hand it is less than 4, the material tested is considered to have a bactericidal effect (Levison, 2004).

2.6 Statistical analysis

The data were presented as means, and the statistical analyses were performed using Microsoft Office Excel, OriginPro 2021 and X'Pert HighScore software.

3. Results and discussion

3.1 Physicochemical Characterization of the clays tested

3.1.1 XRD

✓ **The raw and calcined ghassoul**

The XRD spectrum (**Figure 1**) of the raw ghassoul showed the presence of the phases: stevensite (S), quartz (Q), dolomite (D), and calcite (C). The processing of the spectra by the X'Pert HighScore software with the use of JCPDS (Joint Committee Powder Diffraction Standards), showed the degree positions of the main lines of these phases:

- Stevensite (S) observed at the 2θ =11.56° (Qabaqous *et al*., 2014); 19.32°; 33.15°; 34.74°; and 40.99° (JCPDS: 00-013-0257).
- Dolomite (D) observed at the 2θ = 30.93°; 37.37°; 51.06°; and 59.82° (JCPDS: 00-036-0426).
- Quartz (Q) observed at the 2θ = 20.83°; 26.64°; 39.45°; and 50.16° (JCPDS: 00-005-0490).
- Calcite (C) observed at the 2θ = 29.4°; 35.96° and 43.14°° (JCPDS: 00-005-0586).

The XRD (Figure 1) of ghassoul calcined at 900°C, showed the disappearance of some of these phases and the appearance of new phases:

- Enstatite (E) phase; whose characteristic lines are at 2θ =31.99°; 35.45°; 42.16°; 55.10°; 56.89° and 59.33° (JCPDS : 01-071-0786).
- Diopside phase (d); whose lines are at 2θ =20.31°; 27.77°; 30.12°; 44.73°; 49.93°; and 52.23° (JCPDS : 01-083-1818).

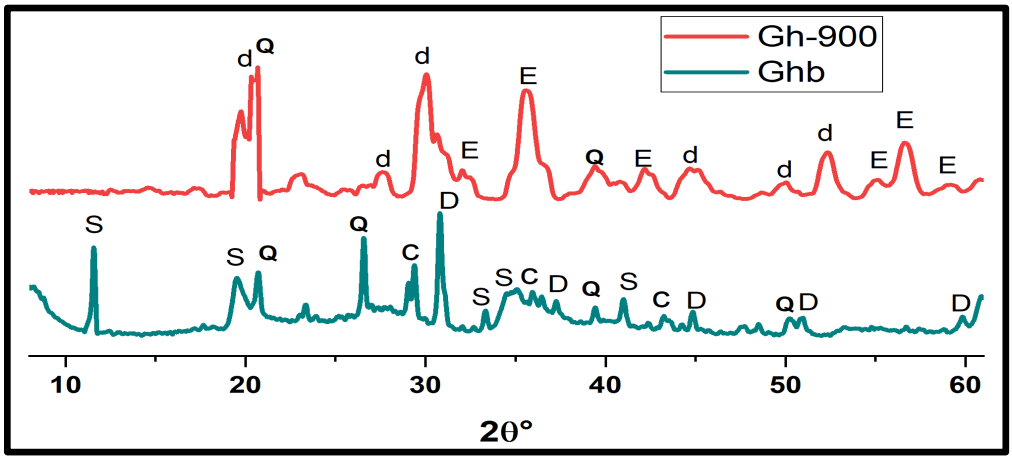

Figure 1. Diffractograms of raw and calcined ghassoul at 900°C

In addition to these new phases appeared, quartz persists, while Stevensite disappears, its absence can be explained by its transformation into Enstatite (Benhammou *et al*., 2009). This transformation can be represented by the following reaction: $Si_4Mg_3(OH)_2O_{10} \rightarrow 3SiMgO_3 + SiO_2 + H_2O$
the other hand, the appearance of diopside ($CaMgSi_2O_6$) can be explained by the following reaction: 1 dolomite+2 quartz= 1 diopside+2CO_2 (Lüttge & Metz, 1993).

✓ **Zn_3Al-CO_3 and Mg_3Al-CO_3**

The diffractograms of Zn_3Al-CO_3 and Mg_3Al-CO_3 (**Figure 2**), show the set of lines (00l) in particular (003), (006), (012), (015), (018), (110) and (113) located respectively at 2θ equal to 11.7°; 23.4°; 34.59°; 39.42°; 46.69°; 60.13°; and 61.60°, which are characteristic of the lamellar structure. These more or less fine and intense lines show the good crystallinity and purity of the sample.

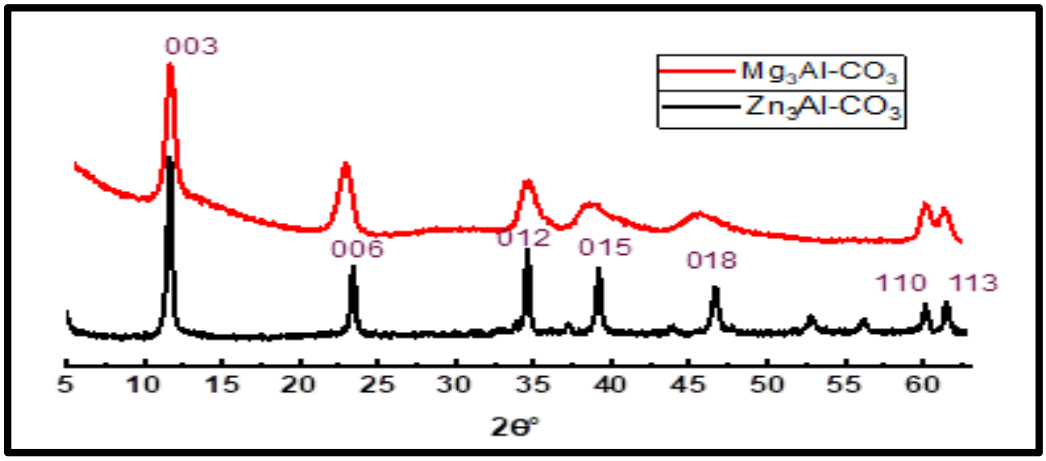

Figure 2. Diffractograms of Zn_3Al-CO_3 and Mg_3Al-CO_3

✓ **Zn_3Al-CO_3 and Mg_3Al-CO_3 calcined**

The diffractograms of Zn_3Al-900 and Mg_3Al-900 (**Figure 3**) show the disappearance of the lines (00l) characteristic of the Hydrotalcite structure. However, new phases appear at 2θ = 31.77°; 34.42°; 36.25°; 47.53°; 56.60°; 62.86°; 66.38°; 67.96° and 69.10° corresponding to zinc oxide (ZnO) (JCPDS: 00-036-1451) and at 2θ =31.24°; 36.84°; 44.81°; 49.07°; 55.66°; 59.34°, 65.23° corresponding to spinel $ZnAl_2O_4$ (JCPDS: 00-005-0669) for hydrotalcite Zn_3Al-CO_3 calcined at 900°C. For Mg_3Al-CO_3 hydrotalcite calcined at 900°C, we observe the appearance of new lines attributed to MgO oxide (JCDS: 00-045-0946) at 2θ = 36.94°; 42.92°; 62.30°, and $MgAl_2O_4$ spinel phase (JCDS: 00-003-0901) at 2θ = 36.96°. However, we note a difference in the position of the characteristic lines of the oxide and spinel phases for the two LDHs, probably due to the nature of the cation constituting the matrix of the material. Moreover, for Zn_3Al-CO_3 the oxide phases are much more developed than in the case of Mg_3Al-CO_3.

3.1.2 Infrared spectroscopy analyses

✓ **The raw and calcined ghassoul**

The IR spectrum (**Figure 4**) of raw Ghassoul (Ghb) showed a band at 3450 cm^{-1} corresponding to the OH stretching vibration of water molecules. The one at 1637 cm^{-1} is attributed to the deformation vibration of water molecules H-OH, while the band at 1450 cm^{-1} corresponds to the elongation vibration CO of carbonates due to the presence of calcite in Ghassoul. In the region 400-1200 cm^{-1}, the thin and intense band at 1020 cm^{-1} is attributed to the elongation vibration of Si-O-Si silica, and the vibrations of (υs (CO_3^{-2})) and Al_2O_3 groups are observed at 880 cm^{-1} (Allaoui *et al*., 2020). For the bands that appear around 666 and 470 cm^{-1}, they are attributed to the vibrations of Si-O-Mg and Si-O-

Si, respectively (Kloprogge *et al*., 2000; Buey, 2000; Anbri *et al*., 2008 ; Basumatary *et al*., 2015 ; Hajjou *et al*., 2020). The absorption band at 794 cm^{-1} is related to the vibration of Fe-OH bonds (Acevedo *et al*., 2017) and that at 730 cm^{-1} corresponds to the CO elongation vibration of carbonates due to the presence of dolomite (Ji *et al*., 2009).

The calcination of ghassoul at 900 °C shows the appearance of the characteristic band of Enstatite (1090 cm^{-1}) (Hajjou *et al*., 2020), and that at 530 cm^{-1} corresponds to the stretching of the MgO group (Kloprogge *et al*., 2000). We also note particularly the disappearance of the band located at 1450 cm^{-1} and the strong decrease in the intensity of the band at 1020 cm^{-1} showing respectively the disappearance of calcite and the pronounced decrease of silica at this temperature. This is in agreement with the observations made by XDR.

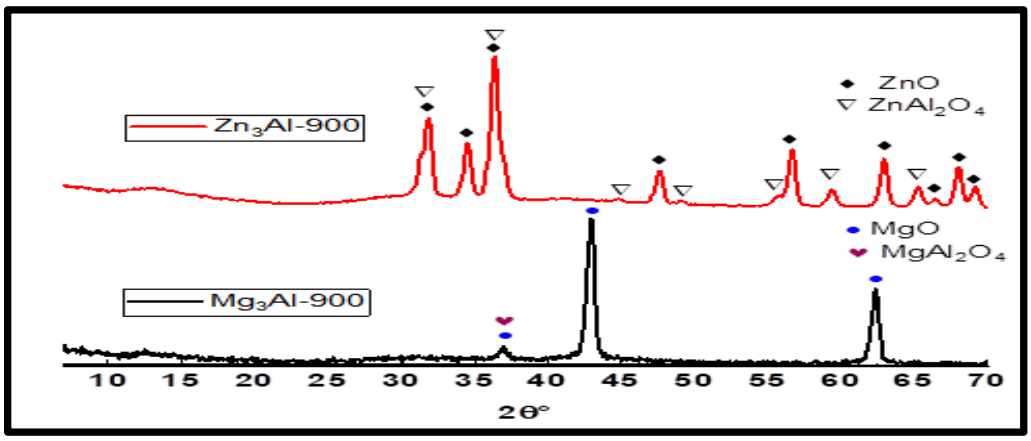

Figure 3. Diffractograms of Zn_3Al-$CO_3$and Mg_3Al-CO_3 calcined at 900°c

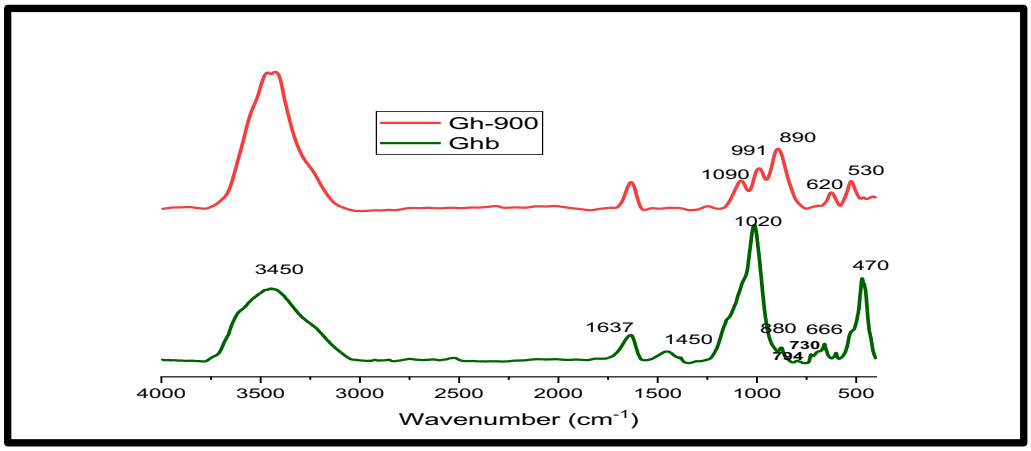

Figure 4. Infrared spectra of raw and calcined Ghassoul at 900°C

✓ **Zn_3Al-CO_3 and Mg_3Al-CO_3 (raw and calcined)**

The spectra of Zn_3Al-CO_3 and Mg_3Al-CO_3 hydrotalcites (**Figure 5**) show a broad and intense band at 3450 cm^{-1} corresponding to the OH stretching vibration of intercalated and physisorbed water molecules(Cheng *et al*., 2010; A. Li *et al*., 2020), accompanied by a band at 1630 cm^{-1} associated with the deformation of water molecules (F. Li *et al*., 2004). he band around 1362 cm^{-1} is attributed to symmetric vibration of $–CO_3^2$ anions (Omonmhenle, 2014) ; (Mahjoubi et al., 2017). There is also the presence of bands located at 428 cm^{-1} and 613 cm^{-1} correspond to Al-OH and OH-Al vibrations respectively (Rong-Chang *et al*., 2015). The band localized at 790 cm^{-1} in the Zn_3Al-CO_3 spectrum corresponds to the characteristic bonding vibration of Zn-OH (Feng *et al*., 2006), while the 850 cm^{-1} band in the Mg_3Al-CO_3 spectrum is attributed to the M-O elongation vibration (Rives, 2001). After

heat treatment at 900°C, the characteristic carbonate band becomes broad and weak and undergoes a shift to 1450 cm^{-1}, which can be explained respectively by the high affinity of MgAl hydrotalcite to carbonates and by the presence of these carbonates in a different environment as for Zn_3Al-900. Also, we note the appearance of new bands at 900 cm^{-1}, 698cm^{-1}, 550 $cm^{-1}$and 510 cm^{-1} corresponding to the Metal-Oxygen-Metal vibrations of the oxide and spinel forms (Fang *et al*., 2002; Wijs *et al*., 2002). Indeed, the bands of vibrations at low frequencies (below 1000 cm^{-1}) are attributed to Metal-Oxygen-Metal bonds (Roelofs *et al*., 2002: Hamouda *et al*., 2016).

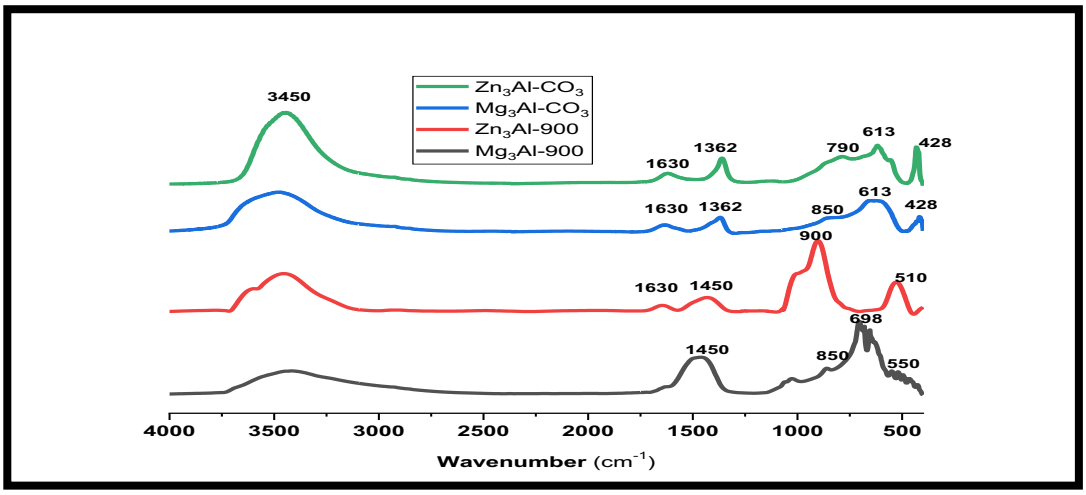

Figure 5. Infrared spectrum of Mg_3Al-CO_3 and Zn_3Al-CO_3 raw and calcined at 900°C

3.1.3 SEM /EDX Analysis

✓ **The raw and calcined ghassoul**

The SEM image of raw Ghassoul (**Figure 6**), indicates that the particles have a petaloid type microstructure, typical of that of smectite clay (Rhouta *et al*., 2008). While the sample calcined at 900 °C has a high porosity and forms particles of different size and shape that coat and bind the grains.

The mass percentage of chemical elements and oxides (**Table 1**), shows that the cationic clay is composed of silicon (26.13%), magnesium (18.36%), calcium (18.3%), iron (10.32%), aluminium (2.47%), potassium (1.21%) and sulphur (0.54%), which correspond respectively in percentage of oxides to 42.72% SiO_2, 20.68% MgO, 20.34% CaO, 10.21% FeO, 3.59% Al_2O_3, 1.2% K_2O, and 1.02% SO_3. These results reveal that it is indeed silicate clay of the smectite type. The important presence of calcium in the raw ghassoul can be explained by its physico-chemical and petrographic characteristics associated with the Miocene carbonate crusts of the Jbel Ghassoul basin (El Faleh, 2001). Following the calcination of ghassoul at 900°C; only silicon, magnesium and potassium were detected, with an increase in percentage of oxides of these elements. This may be due to the transformation of the Stevensite phase into Enstatite (E) and the appearance of the Diopside phase (d), in agreement with the observations made by DRX (**Figure 1**).

✓ **Zn_3 Al-CO_3 raw and calcined**

SEM and EDX of the Zn sample$_3$ Al-CO_3 (**figure 7**), shows small elongated particles that form large agglomerates. Calcination at 900°C leads to the collapse of this morphology and the transformation of the structure into an agglomerated form of small particles probably corresponding to the oxide and spinel forms. The mass percentage of chemical elements and oxides (**Table 2**) showed us that Zn_3 Al-CO_3 consists of the following chemical elements: zinc (51.43%), oxygen (37.41%), and

aluminum (7.52%). In addition, the percentage composition of oxides obtained by SEM is: 76.52% ZnO, and 20.71% Al_2O_3. Following the calcination of Zn_3 Al-CO_3 at 900°C, there is an increase of 16.94% for zinc and 2.01% for aluminum. After heat treatment, there is a percentage increase of 6.77% for the ZnO oxide.

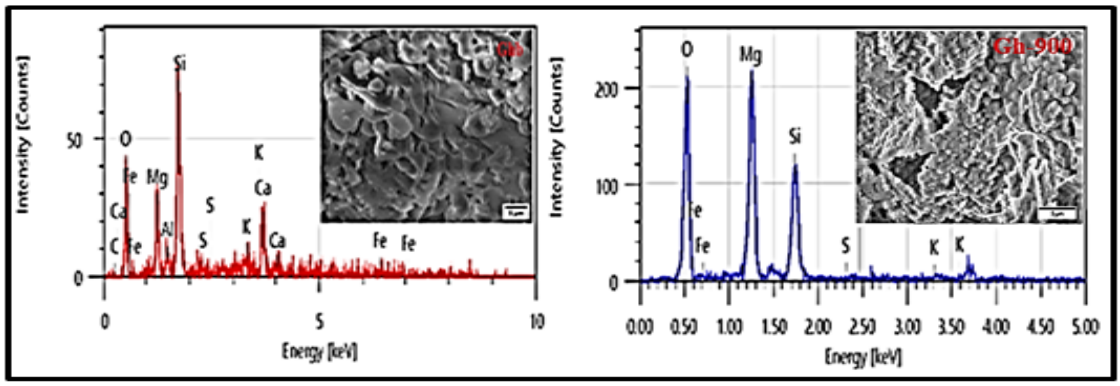

Figure 6. SEM, EDX micrographs of Ghb and Gh-900

Table 1. Elemental composition and percentage of oxide (%) of raw and calcined Ghassoul

	Mass % of chemical elements								
elements	**C**	**O**	**Mg**	**Al**	**If**	**S**	**K**	**It**	**Fe**
Ghb	0.35	22.2	18.36	2.47	26.13	0.54	1.31	18.3	10.32
Gh-900	nd	42.31	30.77	nd	24.18	nd	1.37	nd	nd
	Mass % of oxides								
oxides	**MgO**	**Al_2O_3**	**SiO_2**	**SO_3**	**K_2O**		**CaO**		**FeO**
Ghb	20.68	3.59	42.72	1.01	1.2		20.34		10.21
Gh-900	48.56	nd	48.66	nd	1.55		nd		nd

nd: not detectable

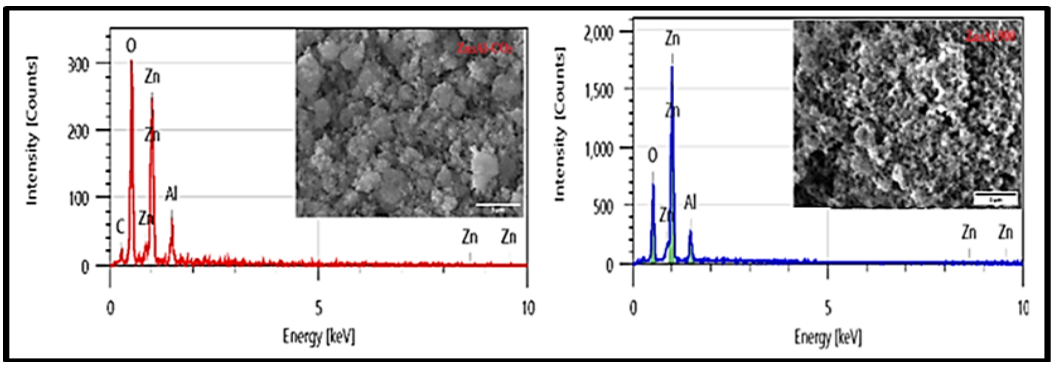

Figure 7. SEM, EDX micrographs of Zn_3 Al-CO_3 and Zn_3 Al-900

Table 2. The percentage of chemical elements and oxides of Zn_3 Al-CO_3 raw and calcined

	% massique des éléments chimiques et des oxydes					
element	**C**	**O**	**Zn**	**Al**	**ZnO**	**Al_2O_3**
Zn_3Al-CO_3	3.64	37.41	51.43	7.52	76	20.71
ZnAl-900	nd	22.10	68.37	9.53	82.77	17.23

nd: not detectable

✓ **Mg_3 Al-CO_3 raw and calcined**

The SEM image obtained (**Figure 8**) for Mg_3 Al-CO_3 shows hydrotalcite particles in the form of parallel sheets with a strong agglomeration, and a platelet morphology, which is in agreement with the typical structure of double lamellar hydroxides. Calcination at 900°C leads to the appearance of an agglomerated structure, of the sand pink type, with the presence of particles of heterogeneous shape and size certainly corresponding to the mixed oxide and spinel. In addition, **Table 3** shows that Mg_3Al-CO_3 consists of the following chemical elements: oxygen (51.70%), magnesium (26.38%), aluminum (11.12%), Chlorine (6.52%), and carbon (4.28%). In addition, the percentage composition of oxides obtained by SEM is: 55.52% MgO, and 28.53% Al_2O_3. Following the calcination of Mg_3 Al-CO_3 at 900°C (**Figure 8**); there is an increase of 30.74%, while aluminum is not detected. This heat treatment resulted in an increase of 44.24% of MgO oxide, and a decrease in percentage of magnesium oxide; almost 100%.

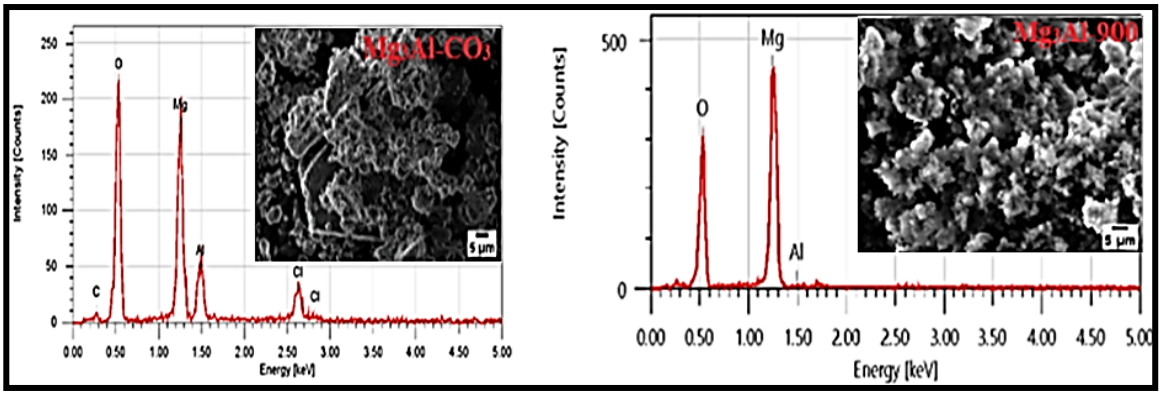

Figure 8. SEM, EDX and chemical element micrographs of Mg_3 Al-CO_3 and Mg_3 Al-900

Table 3. Percentage (%) of Chemical elements and oxides of Mg_3 Al-CO_3 raw and calcined

	Mass % of chemical elements and oxides						
element	**C**	**O**	**Mg**	**Al**	**Cl**	**MgO**	**Al_2O_3**
Mg_3 Al-CO_3	4.28	51.70	26.38	11.12	6.52	55.75	28.53
MgAl-900	nd	42.88	57.12	nd	nd	99.99	0.01

nd: not detectable

3.2 Zero charge point (pH_{zcp})

The measurement of the zero charge point of the materials informs us on the nature of their surface charge, as well as on their behavior towards the contact media. Indeed, when the pH of the solution is lower than the zero charge point, the functional groups on the surface of the material will be protonated by the excess of H^+ ions in the solution and the surface of the clay will be positively charged. On the other hand, if the pH of the solution is higher than the pH_{zcp}, the functional groups on the surface of the adsorbent will be deprotonated by the OH^- ions present in the solution and the surface of the clay will be negatively charged(Kubilay *et al*., 2007; Nandi *et al*., 2009; Hameed, 2009; Karim *et al*., 2010).

Measurement of the zero charge point of the two anionic clays, raw and calcined, showed that the pH_{zcp} of both hydrotalcites increases after calcination at 900°C. It increases from 7.5 for Zn_3Al-CO_3 to 11.4 for Zn_3Al-900, and for Mg_3Al-CO_3 it increases from 7.9 to 10.84 for Mg_3Al-900 (**Figure 9**).

The results of the determination of the zero charge point of the cationic clay (**Figure10**) showed that raw Ghassoul has a basic pH_{zcp} equal to 8.41. Ziyat (2021) found a similar value of 8.48 by potentiometric titration; about the same pH found. While Moussout *et al.*, (2020) found by potentiometric and conductimetric titration with different electrolytes (NaCl, CsCl, NaF, NaBr and LiCl) that the zero charge point of raw ghassoul is located at pH=10.7. This value is higher than the one obtained in this work by the pH drift method, this difference can be attributed to the method used and/or to the initial chemical composition of the material studied.

The measurement of pH_{zcp} of calcined ghassoul (Figure 10) showed a decrease for the latter; its value is equal to 6.95; a more or less neutral pH_{zcp}. This decrease of pH_{zcp} after calcination at 900°C; can be explained by: (i) the change of the ghassoul composition; following the appearance of new mineralogical phases (see XRD), (ii) the disappearance of basic oxides (CaO, FeO) (**Table 1**), (iii) As well as by the ratio (r) of the percentage of acid and basic oxides; $r = \frac{SiO2+SO3}{MgO+CaO+FeO+K2O}$ which is close to unity (0.97), whereas for Ghb this ratio was 0.83 (**Table 1**).

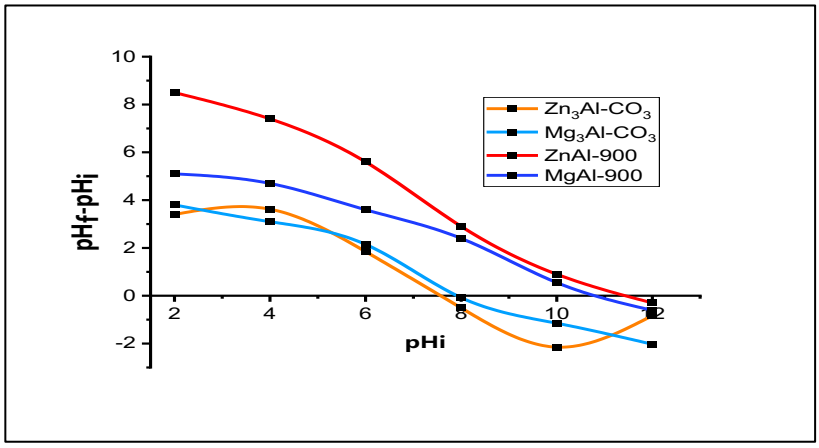

Figure 9. pH_{zcp} of raw and calcined $Zn_3Al\text{-}CO_3$ and $Mg_3Al\text{-}CO_3$

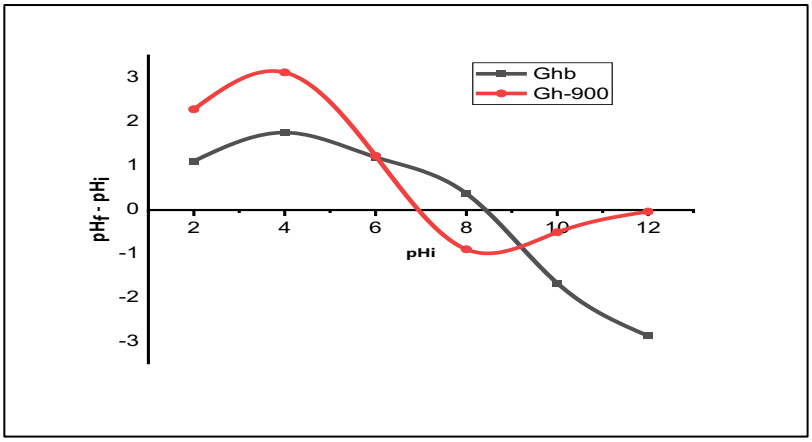

Figure 10. pH_{zcp} of raw and calcined ghassoul

3.3 Bioelectronic coordinates of the studied clays

Following the heat treatment at 900°C, the redox potential (Eh) of the two lamellar double hydroxides decreases significantly. Indeed, Eh of $Zn_3Al\text{-}CO_3$ of value -0. 06V becomes equal to -0.316 V after calcination. Similarly for $Mg_3Al\text{-}CO_3$, its calcination also decreases its redox potential from -0.085 V to -0.209 V. On the contrary, the calcination of ghassoul leads to an increase of its redox potential from -0.103 V to -0.019 V. In addition, the pH of calcined hydrotalcites becomes more basic.

On the other hand, the calcination of ghassoul decreases its pH from 8.75 to a neutral value of 6.95 (**Table 4**). Indeed, the redox potential is a parameter intrinsic to any biological environment, it can intervene at different levels on the microbial cell: gene expression, metabolism, physiology and thus potentially modify its ability to grow (Aubert *et al*., 2002). The calculation of the value of rH2 from the experimental measurement of the Eh potential and the pH, allowed us to evaluate the oxidizing strength of the tested materials, by identifying the only electron transfers. Indeed, the higher the value of rH2, the more it indicates that the system studied has a low concentration of electrons, and is therefore more capable of capturing electrons, and subsequently that the system is more oxidizing (Országh, 1990; Fougerousse, 1996). Thus, the calculation of rH2 for hydrotalcites showed that it increases with calcination. The highest value recorded is for Zn_3Al-900 (rH2=15.15), while rH2 of ghassoul decreased after heat treatment, it goes from 14.04 for Ghb to 13.17 for Gh-900.

Table 4. Bioelectronic coordinates of the studied materials

	rH2	**Eh** (mVolts)	**pH**	**µ** (µS/cm)	**ρ** (ohm.cm)	**Eh²**	**W** (µWatts)
Zn_3Al-CO_3	13.5	-60	7.75	112	8928.6	3600	353
Mg_3Al-CO_3	13.66	-85	8.25	122	8196.7	7225	771
GhB	14.04	-103	8.75	548	1824.8	10609	5087
ZnAl-900	15.15	-316	12.84	7260	137.7	99856	634335
MgAl-900	14.24	-209	10.6	5890	169.8	43681	225121
Gh-900	13.17	-19	6.95	42	23809.5	361	13

The measurement of the power (W) of the studied clays shows that W of Zn_3Al-900 presents the greatest value (0.634Watts), and it is in a state of electrochemical potentiality favorable to dissipate the maximum of energy. On the other hand, this quantity W is in correlation with the evolution of the parameter rH2. The power W is thus all the more important that the system is more oxidizing (rH2 big) (Országh, 1992). Consequently, these measurements of the bioelectronic coordinates allow us to classify the studied clays according to their oxidizing strength (most oxidizing system) by following decreasing order:

ZnAl-900 > MgAl-900 > GhB > Mg_3Al-CO_3 > Zn_3Al-CO_3 > Gh-900

This difference in the oxidizing strength of the materials may be the cause of the difference in their antibacterial power.

The importance of the effect of bioelectronic coordinates on the development of bacteria lies in the change of their optimum which can dramatically affect the growth of bacteria. Therefore, each bacterial species grows in a defined range of pH and Eh. Indeed, neutrophilic bacteria have a pH optimum between 5.5 and 8 (Prescott et al., 2003), case of the tested bacteria. The work of Rabotnova (1963) on the importance of physico-chemical factors (pH and rH2) for the vital activity of bacteria, showed that micro-organisms that have adapted to particular living conditions, the case of pathogenic bacteria, only develop in narrow pH ranges (Rabotnova, 1963).

3.4 Results of the antibacterial test

The antibacterial tests (**Table 5**) carried out on the various materials showed that calcination presents a favorable antibacterial effect in the case of the two double lamellar hydroxides Zn_3Al-CO_3 and Mg_3Al-CO_3 as shown in literature (Dutta *et al*., 2020; Dhanasekaran *et al*., 2017); on the other hand it makes the ghassoul lose its antibacterial power. Indeed, the antibacterial test of the cationic clay calcined at 900°C did not show any antimicrobial effect, whereas in its raw state it showed an antibacterial activity on the tested bacteria.

The bactericidal capacity after heat treatment at 900°C increased by 40% in the case of lamellar double hydroxides for both Gram-positive bacteria. However, in the case of Zn_3Al-CO_3 this antibacterial capacity is much higher (91% for *E. coli* and 80% for *Sal*) compared to Mg_3Al-CO_3 (56% for *E. coli* and 44% for *Sal*). Indeed, the MIC for *Escherichia coli* decreased from 5.6 mg/ml for Zn_3Al-CO_3 to 0.5 mg/ml for Zn_3Al-900, and that of *Salmonella spp* decreased from 5.6 mg/ml for Zn_3Al-CO_3 to 1.1 mg/ml for Zn_3Al-900. For Gram+ bacteria, *Enterococcus feacalis* and *Staphylococcus aureus* the MIC decreased from 6.2 mg/ml to 3.7 mg/ml for calcined Zn_3Al-CO_3.

Similarly for Mg_3Al-CO_3, its antibacterial power increased after calcination (**Table 5**). Indeed, the MIC for *E. coli* decreased from 5 mg/ml for Mg_3Al-CO_3 to 2.2 mg/ml for Mg_3Al-900. While for *Sal* this value decreased from 5 mg/ml for Mg_3Al-CO_3 to 2.8 mg/ml for Mg_3Al-900. For both Gram+ bacteria, the MIC decreased from 6.2 mg/ml to 3.7 mg/ml for Mg_3Al-CO_3 calcined.

In its raw state, ghassoul showed a higher antibacterial efficacy than the two raw hydrotalcites (**Table 5**). While calcination at 900°C of the cationic clay makes it lose its antibacterial power. The same result found by Haydel *et al*., (2008) on the antibacterial effect of the French green clay CsAg02 calcined at 900°C. This suggests that the phases that disappeared after calcination at 900°C (calcite and dolomite) would be responsible for this decrease in antibacterial activity, without ruling out the hypothesis of the Enstatite phase formed following this treatment at 900°C.

Table 5. MIC of the tested materials for the four bacteria

	MIC (mg/ml)			
	S.aureus	***E. F***	***Sal***	***E. coli***
Zn_3Al-CO_3	6.2±0.00	6.2±0.00	5.6±1.4	5.6±1.4
Zn_3Al -900	3.7±1.14	3.7±1.4	1.1±0.4	0.5±0.2
Mg_3Al-CO_3	6.2±0.00	6.2±0.00	5.0±1.7	5.0±1.7
Mg_3Al-900	3.7±1.4	3.7±1.4	2.8±0.7	2.2±0.8
Ghb	5.6±1.4	5.6±1.4	4.3±1.7	3.7±1.4
Gh-900	ANB	ANB	ANB	ANB

ANB : No antibacterial activity for the concentration used (50 mg/ml)

Table 6. BMC and BMC/MIC ratio of tested materials

	Zn_3Al- 900		**Mg_3Al-900**	
	MBC (mg/ml)	**MBC/MIC**	**MBC (mg/ml)**	**MBC/MIC**
S. aureus	5.6	1.5	6.2	1.7
E. F	5.6	1.5	6.2	1.7
Sal	1.4	1.3	4.0	1.4
E. coli	0.6	1.2	2.8	1.3

According to the results (**Table 6**); Zn_3Al-900 and Mg_3Al-900 have bactericidal effect for the four germs tested. The difference in antibacterial activity between Gram-positive and Gram-negative bacteria; can be explained by the type of their outer membrane of the cell envelope, which is composed of phospholipids and lipopolysaccharides that confer a strong negative charge on the cell surface of Gram-negative bacteria. While in Gram positive bacteria, the negative charge is attributed to the presence of teichoic acids; due to the presence of phosphate in their structure.

The increase in bactericidal power of both anionic clays upon calcination at 900°C can be explained by the presence of the oxides Mg-O and Zn-O, the spinel phases $MgAl_2O_4$ and $ZnAl_2O_4$ respectively for Mg_3Al-900 and Zn_3Al 900, as confirmed by XRD and FTIR. The fact that Zn_3Al-900 presents a

higher bactericidal power compared to that of Mg_3Al-900, is related to the nature of the divalent cation (zinc), and the presence of the ZnO phase with good crystallinity and in high proportion, in agreement with the work of Moukrad (2016), who reported that the antimicrobial effect of the studied TiO_2 and ZnO nanoparticles, differs according to their nature, crystalline phase, and morphology. Indeed, zinc induces significant changes in the electrochemical behavior of the calcined ZnAl matrix, since the oxidative-reductive strength of the heat-treated Zn-based materials is higher than that of the calcined Mg-based materials ($rH2_{Zn3Al\text{-}900} > rH2_{Mg3Al\text{-}900}$).

Thus, we can assume that the difference in antibacterial power between clays can be attributed to their surface charge, their pH_{zcp} and their oxidizing or reducing force rH2; which can act on the electrostatic interaction. Thus, the more basic the pH_{zcp} of the material, the more positive the surface charge, and consequently the rH2 and its state of electrochemical potentiality to dissipate energy (the specific power W) is greater. This may explain the high bactericidal power of Zn_3Al-900 material. The chemical composition can also play an important role in the antibacterial power of materials. Certainly the presence of the oxides and the spinel phase favored the increase of the bactericidal power of the two studied hydrotalcites $Mg_3Al\text{-}CO_3$ and Zn_3AlCO_3, but also the nature of the divalent cation has an influence, since the zinc-based material proves to be more active than the Mg-based one. The loss of bactericidal power in Gh-900 can be explained by: i) the ratio (r) of the percentages of acidic and basic oxides, which is close to unity (0.97); ii) the pH_{zcp} (6.95), which is more or less neutral; and iii) the decrease in its oxidizing power. The rH2 of Gh-900 after calcination decreases from 14.04 to 13.17 and the specific power decreases from 5087µWatt to 13µWatt; which can be considered as zero. While the electrochemical potential to dissipate energy for both hydrotalcites after calcination has increased significantly; especially for Zn_3Al-900 (634335 µWatt). Indeed the determination of the maximum power (W) to dissipate energy remains a very relevant parameter to differentiate the bactericidal of the different materials studied.

Conclusion

The study of the antibacterial effect of the anionic clays on the four bacteria tested, showed a considerable effectiveness after calcination of the material at 900°C, in particular the Double Lamellar Hydroxides based on Zn and Mg. The characterization of the different materials used was carried out by XRD, IR and SEM-EDX .Their thermal treatment at 900°C showed changes in their chemical composition and structure. This change resulted in the appearance of oxide and spinel phases. The study of their bioelectronic coordinates (Eh, pH, rH2) showed an increase of their oxidizing character and their basicity following the thermal treatment, and their maximum energy dissipation rate dissipated energy. On the other hand, the calcination at 900°C of the cationic clay "Ghassoul" makes it lose its bactericidal power, which can be attributed mainly to the loss of its specific power of energy dissipation.

We thus deduce that the importance of this study lies in its originality. Indeed, according to our knowledge, it is the first attempt to study the antibacterial power of anionic clays of the double lamellar hydroxide type 'LDH' and cationic clays of the Ghassoul type (natural Moroccan clay) according to the thermal treatment, their bioelectronics coordinates and their chemical characteristics. This work is a contribution to the fight against bacterial resistance to antibiotics, to the maintenance of hygiene of the premises, the depollution of the environment and the valorization of the quality of waste water.

Acknowledgement:

This work is done in the frame work of the project (PPR2), supported by Ministry of National Education, Professional Training for Higher Education and Scientific Research, Morocco (MENFPESRS) and National Center for Scientific and Technical Research/ Rabat, Morocco (CNRST)

Disclosure statement: *Conflict of Interest:* The authors declare that there are no conflicts of interest.
Compliance with Ethical Standards: This article does not contain any studies involving human or animal subjects.

References

Abderrazek K., Najoua F. S., & Srasra E. (2016). Synthesis and characterization of [Zn–Al] LDH: Study of the effect of calcination on the photocatalytic activity. *Applied Clay Science*, *119*, 229–235. https://doi.org/10.1016/j.clay.2015.10.014

Acevedo N. I. A., Rocha M. C. G., & Bertolino L. C. (2017). Mineralogical characterization of natural clays from Brazilian Southeast region for industrial applications. *Cerâmica*, *63*, 253–262.

Ainane A., Taleb M., El-Hajjaji F., Hammouti B., Chetouani A., Ainane T. (2021). Study of dependence between two types of most abundant natural clays in Bejaad province (Central Morocco) using a statistical approach, *Mor. J. Chem.* 9(2), 210-220, https://doi.org/10.48317/IMIST.PRSM/morjchem-v9i2.22438

Allaoui S., Naciri Bennani M., Ziyat H., Qabaqous O., Tijani N., & Ittobane N. (2020). *Kinetic Study of the Adsorption of Polyphenols from Olive Mill Wastewater onto Natural Clay: Ghassoul* [Research Article]. *Journal of Chemistry; Hindawi*. https://doi.org/10.1155/2020/7293189

Anbri Y., Tijani N., Coronas J., Mateo Ester., Menéndez M., & Bentama J. (2008). Clay plane membranes: Development and characterization. *Desalination*, *221*(1), 419–424. doi.org/10.1016/j.desal.2007.01.101

Andrews J. M. (2001). Determination of minimum inhibitory concentrations. *Journal of Antimicrobial Chemotherapy*, *48*(suppl_1), 5–16. https://doi.org/10.1093/jac/48.suppl_1.5

Aubert C., Cappelle N., Jeanson S., Eckert H., Divies C., & Cachon R. (2002). Le potentiel d'oxydoréduction et sa prise en compte dans les procédés d'utilisation des bactéries lactiques. *Sciences Des Aliments - SCI ALIMENT*, *22*, 177–187. https://doi.org/10.3166/sda.22.177-187

Azha S. F., Shamsudin M. S., Shahadat M., & Ismail S. (2018). Low cost zwitterionic adsorbent coating for treatment of anionic and cationic dyes. *Journal of Industrial and Engineering Chemistry*, *67*, 187–198. https://doi.org/10.1016/j.jiec.2018.06.029

Basumatary A. K., Kumar R. V., Ghoshal A. K., & Pugazhenthi G. (2015). Synthesis and characterization of MCM-41-ceramic composite membrane for the separation of chromic acid from aqueous solution. *Journal of Membrane Science*, *475*, 521–532. https://doi.org/10.1016/j.memsci.2014.10.055

Belamine M. (2012). *Le Ghassoul, propriétés cosmétiques et thérapeutiques.* [Thèse du Doctorat en Pharmacie, Université Mohammed V].

Benhammou A., Tanouti B., Nibou L., Yaacoubi A., & Bonnet J.-P. (2009). Mineralogical and Physicochemical Investigation of Mg-Smectite from Jbel Ghassoul, Morocco. *Clays and Clay Minerals*, *57*(2), 264–270. https://doi.org/10.1346/CCMN.2009.0570212

Elyahyaoui A., Ellouzi K., Al Zabadi H.; Razzouki B.; Bouhlassa S.; Azzaoui K.; Mejdoubi E.; Hamed O.; Jodeh S.; Lamhamdi A. (2017). Adsorption of Chromium (VI) on Calcium Phosphate: Mechanisms and Stability Constants of Surface Complexes. *Appl. Sci.*, 7, 222-236, https://doi.org/10.3390/app7030222

Boumchita S., Lahrichi A., Benjelloun Y., Lairini S., Nenov V., & Zerrouq F. (2016). *Elimination d'un colorant cationique dans une solution aqueuse par un déchet alimentaire: Epluchure de pomme de terre [Removal of cationic dye from aqueous solution by a food waste: Potato peel]*. 13.

Buey C. de S. (2000). Mg-Rich Smectite "Precursor" Phase in the Tagus Basin, Spain. *Clays and Clay Minerals*, *48*(3), 366–373. https://doi.org/10.1346/CCMN.2000.0480307

CASFM. (2021). *Comité de l'antibiogramme de la Société Française de Microbiologie, Recommandations 2021, V.1.0 Avril*.

Cavani F., Trifirò F., & Vaccari A. (1991). Hydrotalcite-type anionic clays: Preparation, properties and applications. *Catalysis Today*, *11*(2), 173–301. https://doi.org/10.1016/0920-5861(91)80068-K

Chang Z., Evans D. G., Duan X., Vial C., Ghanbaja J., Prevot V., de Roy M., & Forano C. (2005). Synthesis of [Zn–Al–CO_3] layered double hydroxides by a coprecipitation method under steady-state conditions. *Journal of Solid State Chemistry*, *178*(9), 2766–2777. https://doi.org/10.1016/j.jssc.2005.06.024

Chebaibi A., Marouf Z., RHAZI FILALI F., Fahim M., Ed-Dra A. (2016). Évaluation du pouvoir antimicrobien des huiles essentielles de sept plantes médicinales récoltées au Maroc. *Phytothérapie*, *14*, 355–362. https://doi.org/10.1007/s10298-015-0996-1

Cheng X., Huang X., Wang X., & Sun D. (2010). Influence of calcination on the adsorptive removal of phosphate by Zn–Al layered double hydroxides from excess sludge liquor. *Journal of Hazardous Materials*, *177*(1), 516–523. https://doi.org/10.1016/j.jhazmat.2009.12.063

Crow D. R. (1994). *Principles and Applications of Electrochemistry, 4th Edition (4th ed.)*. *CRC Press*.

Demourgues-Guerlou L., & Delmas C. (1994). Effect of Iron on the Electrochemical Properties of the Nickel Hydroxide Electrode. *Journal of The Electrochemical Society*, *141*(3), 713. https://doi.org/10.1149/1.2054797

Dhanasekaran T., Padmanaban A., Gnanamoorthy G., Manigandan R., Kumar S. P., Stephen A., Selvam P., Subaraja M., and Narayanan V. (2017). Biological Evolution of New Intercalated Layered Double Hydroxides: Anticancer, Antibacterial and Photocatalytic Studies, *ChemistrySelect*, 2, 11717 – 11726 https://doi.org/10.1002/slct.201702621

Dutta S., Jana T. K., Halder S. K., Maiti R., Dutta A., Kumar A., Chatterjee K. (2020). Zn2Al-CO3 Layered Double Hydroxide: Adsorption, Cytotoxicity and Antibacterial Performances, *ChemistrySelect,* 5(20), 6162-6171, https://doi.org/10.1002/slct.202001264

El Faleh E. M. (2001). La croûte zonaire des encroûtements carbonatés tertiaires du bassin de Jbel Rhassoul (Maroc): Caractérisation et mode de formation / Laminar horizon of Tertiary calcretes of the basin of Jbel Rhassoul (Morocco): caracterization and mode of formation. *Géomorphologie : relief, processus, environnement*, *7*(4), 271–279. https://doi.org/10.3406/morfo.2001.1111

Eloff J. (1998). A Sensitive and Quick Microplate Method to Determine the Minimal Inhibitory Concentration of Plant Extracts for Bacteria. *Planta Medica*, *64*(08), 711–713. https://doi.org/10.1055/s-2006-957563

Fang C., Loong C.-K., Wijs G., & With G. (2002). Phonon Spectrum of $ZnAl_2O_4$ Spinel from Inelastic Neutron Scattering and First-Principles Calculations. *Physical Review B*, *66*, 144301. https://doi.org/10.1103/PhysRevB.66.144301

Faure C., Delmas C., & Willmann P. (1991). Electrochemical behavior of α-cobalted nickel hydroxide electrodes. *Journal of Power Sources*, *36*(4), 497–506. https://doi.org/10.1016/0378-7753(91)80075-9

Feng Y., Li D., Wang Y., Evans D. G., & Duan X. (2006). Synthesis and characterization of a UV absorbent-intercalated Zn–Al layered double hydroxide. *Polymer Degradation and Stability*, *91*(4), 789–794. https://doi.org/10.1016/j.polymdegradstab.2005.06.006

Fougerousse A. (1996). Le potentiel redox E et le rH2 deux approches de l'évaluation de la force des oxydants et des réducteurs. *Bull. Union Phys*, *90*, 319–331.

Hajjou H., Benlhachemi A., Saâdi L., & Waqif M. (2020). Reactive sintering behavior of Moroccan clay "Ghassoul." *Materials Today: Proceedings*, *22*, 112–119. https://doi.org/10.1016/j.matpr.2019.08.109

Hameed B. H. (2009). Evaluation of papaya seeds as a novel non-conventional low-cost adsorbent for removal of methylene blue. *J. Hazard. Mater.*, *162*(2), 939–944. doi.org/10.1016/j.jhazmat.2008.05.120

Hamouda S., Bouteraa S., Bahmani A., & Bettahar N. (2016). Les hydrotalcites et leurs applications dans l'environnement. *algerian journal of environmental science and technology*, *2*(3), 55–61.

Haydel S. E., Remenih C. M., & Williams L. B. (2008). Broad-spectrum in vitro antibacterial activities of clay minerals against antibiotic-susceptible and antibiotic-resistant bacterial pathogens. *Journal of Antimicrobial Chemotherapy*, *61*(2), 353–361. https://doi.org/10.1093/jac/dkm468

Jahanpanahi M. (2016). Antimicrobial effect of nanofluid including Zinc oxide (ZnO) nanoparticles and Mentha pulegium essential oil. *Journal of Applied Biology and Biotechnology*, 085–089. https://doi.org/10.7324/JABB.2016.40410

Ji J., Ge Y., Balsam W., Damuth J. E., & Chen J. (2009). Rapid identification of dolomite using a Fourier Transform Infrared Spectrophotometer (FTIR): A fast method for identifying Heinrich events in IODP Site U1308. *Marine Geology*, *258*(1–4), 60–68. https://doi.org/10.1016/j.margeo.2008.11.007

Karim A., Mounir B., Hachkar M., Bakasse M., & Yaacoubi A. (2010). Élimination du colorant basique « Bleu de Méthylène » en solution aqueuse par l'argile de Safi. *Revue des sciences de l'eau / Journal of Water Science*, *23*(4), 375–388. https://doi.org/10.7202/045099ar

Kim S. S., Zhang W., & Pinnavaia T. J. (1998). Ultrastable Mesostructured Silica Vesicles, *Science, 282*(5392), 1302–1305, https://doi.org/10.1126/science.282.5392.1302

Kloprogge J. T., Frost R. L., Hickey L. (2000). Infrared emission spectroscopic study of the dehydroxylation of some hectorites. *Thermochimica Acta*, *345*(2), 145–156. https://doi.org/10.1016/S0040-6031(99)00359-7

Kubilay Ş., Gürkan R., Savran A., & Şahan T. (2007). Removal of Cu(II), Zn(II) and Co(II) ions from aqueous solutions by adsorption onto natural bentonite. *Adsorption*, *13*(1), 41–51. https://doi.org/10.1007/s10450-007-9003-y

Levison M. E. (2004). Pharmacodynamics of antimicrobial drugs. *Infectious Disease Clinics of North America*, *18*(3), 451–465. https://doi.org/10.1016/j.idc.2004.04.012

Li A., Deng H., Ye C., & Jiang Y. (2020). Fabrication and Characterization of Novel ZnAl-Layered Double Hydroxide for the Superadsorption of Organic Contaminants from Wastewater. *ACS Omega*, *5*(25), 15152–15161. https://doi.org/10.1021/acsomega.0c01092

Li F., Zhang L., Evans D. G., Forano C., & Duan X. (2004). Structure and thermal evolution of Mg–Al layered double hydroxide containing interlayer organic glyphosate anions. *Thermochimica Acta*, *424*(1), 15–23. https://doi.org/10.1016/j.tca.2004.05.007

Longchambon L. (1939). Recherches sur les propriétés physico-chimiques des argiles kaoliniques. *Bulletin de la Société française de Minéralogie*, *62*(1), 5–88. https://doi.org/10.3406/bulmi.1939.4458

Lüttge A., & Metz P. (1993). Mechanism and kinetics of the reaction: 1 dolomite + 2 quartz = 1 diopside + 2 CO2: a comparison of rock-sample and of powder experiments. *Contributions to Mineralogy and Petrology*, *115*(2), 155–164. https://doi.org/10.1007/BF00321217

Mahjoubi F. Z., Khalidi A., Abdennouri M., & Barka N. (2017). Zn–Al layered double hydroxides intercalated with carbonate, nitrate, chloride and sulphate ions: Synthesis, characterisation and dye removal properties. *Journal of Taibah University for Science*, *11*(1), 90–100. https://doi.org/10.1016/j.jtusci.2015.10.007

Miyata S. (1975). The Syntheses of Hydrotalcite-Like Compounds and Their Structures and Physico-Chemical Properties—I: The Systems Mg^{2+}-Al^{3+}-NO_3^-, Mg^{2+}-Al^{3+}-Cl^-, Mg^{2+}-Al^{3+}-ClO_4^-, Ni^{2+}-Al^{3+}-Cl^- and Zn^{2+}-Al^{3+}-Cl^-. *Clays and Clay Minerals*, *23*(5), 369–375. https://doi.org/10.1346/CCMN.1975.0230508

Moukrad N. (2016). *Etude in vitro de l'effet des nanoparticules des oxydes métalliques TiO_2 et ZnO et mixtes synthétisées à partir de différents précurseurs pour ZnO sur des cellules procaryotes et eucaryotes.* [Thèse de Doctorat]. Université Moulay Ismail.

Moussout H., Ahlafi H., Aazza M., Chfaira R., & Mounir C. (2020). Interfacial electrochemical properties of natural Moroccan Ghassoul (stevensite) clay in aqueous suspension. *Heliyon*, *6*(3), e03634. https://doi.org/10.1016/j.heliyon.2020.e03634

Nandi B. K., Goswami A., & Purkait M. K. (2009). Adsorption characteristics of brilliant green dye on kaolin. *Journal of Hazardous Materials*, *161*(1), 387–395. https://doi.org/10.1016/j.jhazmat.2008.03.110

Nawal D. (2015). *Hydroxydes doubles lamellaires, synthèse, caractérisation et propriétés* [Thèse, Université Sorbonne Paris Cité]. https://tel.archives-ouvertes.fr/tel-01488539/document

Newman S. P., & Jones W. (1999). Comparative Study of Some Layered Hydroxide Salts Containing Exchangeable Interlayer Anions. *Journal of Solid State Chemistry*, *148*(1), 26–40. https://doi.org/10.1006/jssc.1999.8330

Olivier H., Husson B., Brunet A., Babre D., Alar K., Sarthou J.-P., Charpentier H., Durand M., Benada J., & Henry M. (2015). Practical improvements in soil redox potential (Eh) measurement for characterisation

of soil properties. Application for comparison of conventional and conservation agriculture cropping systems. *Analytica Chimica Acta*, *906*, 98–109. https://doi.org/10.1016/j.aca.2015.11.052

Omonmhenle S. I. (2014). Intercalation of anionic surfactants into Zn-Al hydrotalcites of varying composition: preparation and characterisation, *Nigerian Journal of Materials Science and Engineering*. *5*(1), 7.

Országh J. (1990). Vers une approche théorique et expérimentale plus cohérente. *Sciences du Vivant*, *1*, 23–34.

Országh J. (1992). Quelques aspects physico-chimiques des coordonnées bioélectroniques. *Sciences du vivant*, *4*, 45–62.

Prescott L.-M., Harley J., Klein D.-A., Bacq-Calberg C.-M., & Dusart J. (2003). *Microbiologie* (2e édition). *De Boeck*.

Qabaqous O., Bennani M. N., Tijani N., Ziyat H., & Arhzaf S. (2018). Removal of hexavalent Chromium by Ghassoul Hydrotalcites Membranes (GHTM). *J. Mater. Environ. Sci*, *9*(9), 2511–2519.

Qabaqous O., Tijani N., Bennani M. N., & EL Krouk A. (2014). Elaboration et caractérisation des supports plans à base d'argile (Rhassoul) pour membranes minérales. *J. Mater. Environ. Sci*, *5*(1), 2244–2249.

Rabotnova I. L. (1963). The importance of physical-chemical factors (pH and rH2) for the life activity of microorganisms. *ARMY BIOLOGICAL LABS FREDERICK MD*, 303.

Rasouli N., Movahedi M., & Doudi M. (2017). Synthesis and characterization of inorganic mixed metal oxide nanoparticles derived from Zn–Al layered double hydroxide and their antibacterial activity. *Surfaces and Interfaces*, *6*, 110–115. https://doi.org/10.1016/j.surfin.2016.11.007

Reichle W. T. (1986). Synthesis of anionic clay minerals (mixed metal hydroxides, hydrotalcite). *Solid State Ionics*, *22*(1), 135–141. https://doi.org/10.1016/0167-2738(86)90067-6

Rhouta B., Kaddami H., Elbarqy J., Amjoud M., Daoudi L., Maury F., Senocq F., Maazouz A., & Gerard J.-F. (2008). Elucidating the crystal-chemistry of Jbel Rhassoul stevensite (Morocco) by advanced analytical techniques. *Clay Minerals*, *43*(3), 393–403. https://doi.org/10.1180/claymin.2008.043.3.05

Rives V. (2001). *Layered Double Hydroxides: Present and Future*. Nova Publishers, New York.

Roelofs J. C. A. A., van Bokhoven J. A., van Dillen A. J., Geus J. W., & de Jong K. P. (2002). The Thermal Decomposition of Mg-Al Hydrotalcites: Effects of Interlayer Anions and Characteristics of the Final Structure. *Chemistry - A European Journal*, *8*(24), 5571–5579. https://doi.org/10.1002/1521-3765(20021216)8:24<5571::AID-CHEM5571>3.0.CO;2-R

Rong-Chang Z., Xiao-Ting L., Zhen-Guo L., Fen Z., Shuo-Qi L., & Hong-Zhi C. (2015). Corrosion resistance of Zn–Al layered double hydroxide/ poly(lactic acid) composite coating on magnesium alloy AZ31. *Frontiers of Materials Science*, *9*(4), 355–365. https://doi.org/10.1007/s11706-015-0307-7

Sahoo S., Uma Banerjee S., & Sharma Y. C. (2014). Application of natural clay as a potential adsorbent for the removal of a toxic dye from aqueous solutions. *Desalination and Water Treatment*, *52*(34–36), 6703–6711. https://doi.org/10.1080/19443994.2013.816872

Shah I., Adnan R., Wan Ngah W. S., & Mohamed N. (2015). Iron Impregnated Activated Carbon as an Efficient Adsorbent for the Removal of Methylene Blue: Regeneration and Kinetics Studies. *PLoS ONE*, *10*(4), e0122603. https://doi.org/10.1371/journal.pone.0122603

Thenevot F., Szymanski R., & Chaumette P. (1989). Preparation and caracterization of A1-RICH Zn-A1 Hydrotalcite- like compounds. *Clays and Clay Minerals*, *37*(5), 396–402. https://doi.org/10.1346/CCMN.1989.0370502

Toraishi T., Nagasaki S., & Tanaka S. (2002). Adsorption behavior of IO_3^- by CO_3^{2-}- and NO_3^--hydrotalcite. *Applied Clay Science*, *22*(1–2), 17–23. https://doi.org/10.1016/S0169-1317(02)00108-4

Vaccari A. (1998). Preparation and catalytic properties of cationic and anionic clays. *Catalysis Today*, *41*(1–3), 53–71. https://doi.org/10.1016/S0920-5861(98)00038-8

Velu S., Ramkumar V., Narayanan A., & Swamy C. S. (1997). Effect of interlayer anions on the physicochemical properties of zinc–aluminium hydrotalcite-like compounds. *Journal of Materials Science*, *32*(4), 957–964. https://doi.org/10.1023/A:1018561918863

Wade D., Silveira A., Rollins-Smith L., Bergman T., Silberring J., & Lankinen H. (2001). Hematological and antifungal properties of temporin A and a cecropin A-temporin A hybrid. *Acta Biochimica Polonica*, *48*(4), 1185–1189.

Wijs G., Fang C., Kresse G., & With G. (2002). First-principles calculation of the phonon spectrum of $MgAl_2O_4$ spinel. *Physical Review B*, *65*, 094305. https://doi.org/10.1103/PhysRevB.65.094305

Zegaoui O., Moukrad N., Daou I., Filali F. R., Louazri L., & Ahlafi H. (2014). Study of the influence of the shape and size of the ZnO nanoparticles synthesized from different precursors on the antibacterial activity. *Journal of Advances in Chemistry*, *10*(2), 9.

Zerhouni J., Filali F. R., Bennani M. N., Qabaqous O., Houssaini J., Allaoui S., & Benhallam F. (2021). Study of the Effect of Acid-base Character of the Lamellar Double Hydroxides "Zn_3Al-CO_3" and of the "Ghassoul" Clay on their Redox Potential and Antimicrobial Activities. *Iranian Journal of Materials Science and Engineering*, *18*(4), 13. DOI: 10.22068/ijmse.2202

Zerhouni J., Qabaqous O., Filali F. R., Bennani M. N., & Tijani N. (2019). Performance study of the membrane Based layered double hydroxides 'ZnAl-Gh' In The purification of groundwater. *Karbala International Journal of Modern Science*, *5*(4), 12. https://doi.org/10.33640/2405-609X.1148

Ziyat H. (2021). *Élaboration de formulation argile/huile essentielle: Application pour usage fongicide* [Thèse de Doctorat]. Université Moulay Ismail.